


RESEARCH

Open Access



Flow velocity and nutrients affect CO₂ emissions from agricultural drainage channels in the North China Plain

Peifang Leng^{1,2,3}, Fadong Li^{1,3*} , Kun Du^{1,3}, Zhao Li^{1,3}, Congke Gu^{1,3} and Matthias Koschorreck²

Abstract

Background: Groundwater is typically over-saturated in CO₂ with respect to atmospheric equilibrium. Irrigation with groundwater is a common agricultural practice in many countries, but little is known about the fate of dissolved inorganic carbon (DIC) in irrigation groundwater and its contribution to the CO₂ emission inventory from land to the atmosphere. We performed a mesocosm experiment to study the fate of DIC entering agricultural drainage channels in the North China Plain. Specifically, we aimed to unravel the effect of flow velocity and nutrient on CO₂ emissions.

Results: All treatments were emitting CO₂. Approximately half of the DIC in the water was consumed by TOC production (1–16%), emitted to the atmosphere (14–20%), or precipitated as calcite (CaCO₃) (14–20%). We found that DIC depletion was stimulated by nutrient addition, whereas more CO₂ evasion occurred in the treatments without nutrients addition. On the other hand, about 50% of CO₂ was emitted within the first 50 h under high flow velocity. Thus, in the short term, high nutrient levels may counteract CO₂ emissions from drainage channels, whereas the final fate of the produced biomass (burial versus mineralization to CO₂ or even CH₄) determines the duration of the effect.

Conclusion: Our study reveals that both hydrology and biological processes affect CO₂ emissions from groundwater irrigation channels. The estimated CO₂ emission from total groundwater depletion in the North China Plain is up to 0.52 ± 0.07 Mt CO₂ year⁻¹. Thus, CO₂ emissions from groundwater irrigation should be considered in regional CO₂ budgets, especially given that groundwater depletion is expected to acceleration in the future.

Keywords: CO₂ emissions, Agricultural irrigation drainage, Controlled experiments, Groundwater, North China Plain

Background

Groundwater is a critical water resource around the globe ensuring food and water security [1]. Irrigation with groundwater for agricultural activities is a common practice in many arid and semi-arid regions [2]. However, over exploitation of groundwater has led to severe groundwater depletion in several regions of the world [3]. Areas most affected by groundwater depletion are California and Midwest in the US, Northern India, and the

North China Plain (NCP) [4]. In the NCP approximately 70% of the irrigated area is currently groundwater-fed [5, 6] which causes the groundwater level to drop by more than 2 cm per year [7]. While several studies focus on the importance and influence of the dramatic groundwater level drop, the further fate of the pumped irrigation water is much less studied [8].

Groundwater is typically 10- to 100-fold over-saturated with CO₂ [9], even up to 250 times the atmospheric equilibrium value [10]. Thus, if it is pumped to the surface, CO₂ is released. First estimates show that CO₂ emissions from groundwater pumping probably represent a globally significant source of CO₂ [11], with both CO₂ liberation from the water and CO₂ production due to pump energy generation contributing to

*Correspondence: lifadong@igsnr.ac.cn

¹ Key Laboratory of Ecosystem Network Observation and Modeling, Institute of Geographic and Natural Resources Research, Chinese Academy of Sciences, Beijing, China
Full list of author information is available at the end of the article

the negative climate impact of groundwater irrigation [12]. CO₂ has been recognized as the dominant driver of climate change resulting in tremendous deteriorative impacts on the environment and society at a global scale [13]. As one of the major emission sources of CO₂, agricultural land plays an important role in the global carbon cycle [14]. Direct CO₂ emissions from agriculture have been well-documented in many regions [15–17]. However, indirect emission sources, such as irrigation drainages and rivers receiving drainage water, may account for a large part of the uncertainties in the carbon budgets of agricultural ecosystems [18–21].

If CO₂ containing water equilibrates with the atmosphere, not only the dissolved CO₂ but also other species of the carbonate system have to be considered [22]. Existing estimates of CO₂ emissions from groundwater pumping assume complete evaporation of the pumped water, leaving solutes and solids at the surface. Under such conditions, each molecule of CO₂ outgassing is theoretically produced from two molecule of carbonate hardness (refers to HCO₃⁻ + CO₃²⁻) to re-equilibrate with atmospheric CO₂ accompanied by one molecule of carbonate precipitation simultaneously [11, 23]. Thus, maximum CO₂ liberation from groundwater dissolved inorganic carbon could be calculated from the bicarbonate content of the groundwater [9]. When a large part of dissolved inorganic carbon (DIC) containing irrigation water drains into surface waters, DIC may have four different fates: evasion as CO₂, carbonate precipitation, fixation into biomass by TOC production, and downstream transport [24].

Streams are recognized as important CO₂ sources to the atmosphere [25, 26]. In streams the distribution among the four fates of groundwater inorganic carbon is controlled by both hydrological and biochemical processes and their complex interactions [10, 27]. Flow velocity, characterized by fluctuating hydraulic conditions due to flood irrigation or excessive utilization of water resources, usually results in enhanced carbon export from terrestrial and wetland habitats to fluvial networks that subsequently become a source of CO₂ [25, 28, 29]. Turbulence at the air–water interface, which is dependent on the river geomorphology and the river flow, affects the gas transfer coefficient of CO₂, which ultimately determines fluvial CO₂ emissions [30–32]. On the other hand, increasing nutrient levels stimulate biological processes such as algal growth, which decrease DIC concentration by converting CO₂ to organic carbon via photosynthesis [33]. Agricultural drainage water is typically high in inorganic nutrients. Thus, our hypothesis is that both nutrients and flow velocity mediate the relative importance of uptake versus outgassing of CO₂ accompanied with calcite precipitation from the dense

agricultural drainage channels transporting pumping groundwater.

However, quantifying these processes of DIC depletion remains challenging. It is difficult to disentangle the effects of both factors on the fate of inorganic carbon from field observations only, primarily due to uncontrolled environmental conditions. We, therefore, performed a mesocosm experiment in the field to explore how CO₂ emissions from irrigation groundwater respond to nutrients and flow velocity treatments. The goals of this study are to (1) quantitatively testify the effects of nutrients and flow velocity on CO₂ emissions and the carbon budget of irrigation drainage channels in a typical agricultural region in China, and (2) provide implications to CO₂ emission potential from the irrigation groundwater in the NCP as well as other similar regions worldwide.

Methods

Study area

Our study was conducted in the Yucheng Comprehensive Experiment Station of Dezhou Irrigation District (DID) between 115°45′–117°36′ E and 36°24′–38°00′ N, located in the North China Plain. The annual-averaged precipitation is 587 mm (ranges from 286 to 1034 mm). Precipitation occurs mostly from June to September, which accounts for 75% of the total annual amount. Annual evaporation is between 900 and 1400 mm and annual mean temperature is 12.8 °C [34]. The groundwater for agricultural irrigation is characterized by high alkalinity and enriched with agricultural nutrients when it enters the drainage channels [35]. Groundwater bicarbonate concentrations in the NCP can range between 1.55 and 7.65 mmol L⁻¹ [36]. The ditches and canals are mainly artificial and lined with concrete.

Historically, DID has been characterized by anthropogenic activities, particularly intensive agriculture development, which has been causing a high demand of water resources in the NCP [37]. Irrigation drainages were built during the twentieth century to increase crop yield in the salinized soil by diverting water from the lower reaches of the Yellow River to DID. Given that the surface water cannot fulfill the demand from agricultural and industrial production, over-exploitation of groundwater had been frequently observed through the sharp decrease of the groundwater table and heavy pollution therein [38]. To eliminate the influence of soil salinity on crop growth, flooding irrigation is still commonly applied among local farmers. This enhances nutrient inputs from irrigated groundwater into the surface water network that subsequently become a source of CO₂. Based on farmer's practice when they irrigate the crops, our experiment simulate that stream drainage collected from groundwater-irrigated agricultural land. For better representation

of local groundwater, we used groundwater from a local irrigation well as inlet water to our experimental system.

Mesocosm setup

Cubic mesocosms (volume 0.2 m³) were constructed to mimic drainage channels. The physical design of our mesocosms follows that from Petersen et al. [39]. The systems are composed of sixteen cuboid polyvinyl chloride plastic tanks with 0.9 m in length, 0.3 m in width, and 0.6 m in depth. Depth of water was set to 0.5 m. Mesocosms were placed outdoor and remained open and in contact with the field atmosphere to ensure natural light and weather conditions. The containers were sunk into the ground to buffer heating from ambient atmosphere temperature and solar radiation. The electrical wiring for power supplying was also buried. The upper edge of the tanks was 10 cm above the ground so that no surface runoff could flow into containers during rainstorms. The containers allow a factorial design combining two nutrient levels with two flow velocity levels in four replicates (Additional file 1: Figure S1). The tanks were equipped with two alternative submerged pumps to mimic river flowing. Each mesocosm had an individual pump (65 W or 15 W) to provide continuous flowing condition and to preclude water pressure differences of connected pipes when sharing the same pump under the same treatment. The pumps were placed in mesh cages to prevent snails, insects, and floating fragments from suction into the pump and to reduce the risk of clogging. The inlet of the pump was on the shorter side of the tank to simulate a unit of water channel (Fig. 1). We set the length to width ratio as 3:1 to establish a realistic flow regime in the

central part of our setting. The middle section along the longitudinal direction of these tanks can be considered a homogeneous flow field with simple physical boundaries.

Experimental procedure

Groundwater was collected from a nearby agricultural irrigation well from a depth of 5 m and pumped into the pre-cleaned tanks without sediments. Nutrients were added into the tanks at the beginning of the experiment for the high-nutrient treatment, while low-nutrient tanks received no additional nutrients. Particularly, high-nutrient tanks were instantaneously fed with 40 mg P m⁻³ and 4000 mg N m⁻³ as K₂HPO₄ and Ca(NO₃)₂, respectively. We set the nutrient enrichment level by mimicking the two alternative states existing in the local drainage system. The nitrate and ammonia concentrations of the study groundwater well were approximately 0.02 mg N L⁻¹ and 5.8 μg N L⁻¹, respectively, while the nitrate concentration of drainages in a field survey in Yucheng (on 16th and 17th of September) varied from 0.02 to 0.42 mg N L⁻¹ with a mean value of 0.17 mg N L⁻¹ (Table 1). Other parameters in the experimental water were comparable to that in the surface water as well (Table 1). We designed the initial nitrate concentration for the high nutrient experimental group at a level above the average nitrate concentration (0.3 mg N L⁻¹). Phosphorous was added with the N:P molar ratio of 10:1 following Lone et al. [40].

We choose flow velocities in surrounding drainage channels as a reference. Flow velocity of local drainages varied from 0.001 to 0.340 m s⁻¹ during our field sampling. Accordingly, two levels of flow velocity were set to 0.1 and 0.4 m s⁻¹. Pumps were cleaned manually every 3 days. It is expected that there was little CO₂ degassing through pumping itself, since the submerged pumps were tested for air-tightness before usage and it is expected that any artifact would be equal between low and high nutrient treatments, because the same pumps were used.

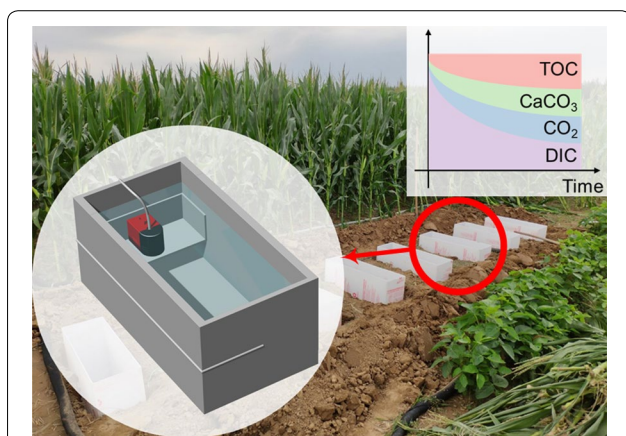


Fig. 1 Conceptual diagram of a single container with a pump. The up-right insert panel shows a conceptual model of DIC transformation in the mesocosm. The fate of DIC was categorized into four pathways: CO₂ evasion, TOC production, calcite precipitation, and downstream transport

Table 1 Characteristics of the groundwater and surface water in the study area

Parameter	Unit	Groundwater	Surface water
pH	–	7.31 ± 0.13	7.06 ± 4.13
Alkalinity	mmol L ⁻¹	785 ± 123	–
DIC	mg L ⁻¹	–	3.83 ± 1.30
NO ₃ ⁻ -N	mg L ⁻¹	0.02 ± 0.01	0.17 ± 0.10
NH ₄ ⁺ -N	μg L ⁻¹	5.8 ± 1.1	3.2 ± 5.8

pH and alkalinity data in the groundwater were from Li et al. [42], NO₃⁻-N and NH₄⁺-N data in groundwater were from this study; pH, DIC, NO₃⁻-N, and NH₄⁺-N data in surface water were unpublished from the field survey in September, 2018

Overall, there were four (2×2) treatments with 4 replicates each in our experimental design, which are denoted as: high nutrient and high flow velocity (A + H); high nutrient and low flow velocity (A + L); low nutrient and high flow velocity (N + H); and low nutrient and low flow velocity (N + L).

The experiments were conducted between 31st August and 15th September 2018. Sampling and measurements of the physical and chemical parameters were performed at 0, 4, 16, 32, 64, 112, 160, 280 h. The experiment measurement was finished after 12 days when the CO_2 concentration had reached equilibrium with the atmosphere. Due to the mesocosm malfunction, the N + H treatment has only one replicate after 50 h.

Sampling and analysis

Water temperature, dissolved oxygen (DO), and electrical conductivity (EC) were measured using multi-parameter probes (Hach H40d, USA). Water level and flow velocity were recorded using a flow meter (HR-2, China) in parallel to each sampling. Water samples were collected to quantify concentrations of nitrate, ammonium, DIC, alkalinity, and TOC. For determination of NO_3^- -N and NH_4^+ -N concentration, water samples were filtered using 0.45 μm filters by spectrophotometry (TU-1810DSPC, China). Calibration curves were produced using reference samples according to quality control standards and were then applied to evaluate data from each set of samples. Reagents, procedural blanks, and samples were measured twice in parallel, with average values reported. The differences between two replicates were within 5% of the mean value for all samples. NO_3^- and NH_4^+ concentrations could be measured at precisions of 2.6% and 8.6%, respectively. DIC and TOC were analyzed with a Vario TOC Analyzer (Elementar Analysensysteme GmbH, Germany). The detection limits of DIC and TOC were 4 and 1 $\mu\text{g L}^{-1}$ with precisions of 1.5% and 5%, respectively. Alkalinity was determined by titration with ~ 0.01 M H_2SO_4 at a precision of 6%. While the measured TOC data could not be directly used. We used two methods to quantify CO_2 emissions during our experiments: a carbon budget approach and direct flux measurements using floating chambers (see Additional file 1 for method details).

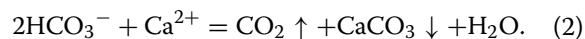
Calculation of C budgets

Changes of DIC in the mesocosms can be separated into three parts: carbon dioxide evasion, calcite precipitation, and total organic carbon (TOC) production (Fig. 1):

$$\Delta\text{DIC} = \Delta\text{CO}_2 + \Delta\text{CaCO}_3 + \Delta\text{TOC}. \quad (1)$$

To verify whether carbonate precipitation was likely to occur within the mesocosm, we calculated calcite

saturation indices (SIs) using PHREEQC [41]. Because we did not measure calcium concentrations in the mesocosm, we used historical rainy season data from irrigation ditches in Dezhou District [42] and derived possible SIs with 1.28 ± 0.16 (mean value \pm standard deviation). Therefore, we assumed calcite precipitation occurred in all mesocosms, with 1 mol each of CO_2 outgassed and CaCO_3 precipitated from 2 mol of HCO_3^- according to Wood and Hyndman [11]:



CO_2 evasion depends on CO_2 concentration and the physical gas transfer velocity [32]. The CO_2 concentration is affected by the thermodynamic carbonate equilibrium. TOC formation is a biological process that converts inorganic carbon into organic matter. At any time, the variation for DIC is denoted as:

$$\text{DIC}_0 - \text{DIC}_t = \Delta\text{CO}_2 + \Delta\text{CaCO}_3 + (\text{TOC}_t - \text{TOC}_0). \quad (3)$$

Equation (3) is based on our hypothesis that CO_2 in the system was over-saturated and TOC was generated during the experiment, DIC_0 and TOC_0 is the amount of DIC and TOC at the initial time, respectively, and DIC_t and TOC_t is the amount of DIC and TOC at time t , respectively. ΔCO_2 and ΔCaCO_3 is the amount of CO_2 outgassing and calcite precipitating during time 0 to time t , respectively. Combined with Eq. (2),

$$\Delta\text{CO}_2 = \Delta\text{CaCO}_3. \quad (4)$$

This is a conservative estimate as we note that the ratio of $\Delta\text{CO}_2 : \Delta\text{CaCO}_3$ can range from 1.18 to 1.88 [9]. The CO_2 evasion could be deduced by the difference between the variation amount of DIC and the variation amount of TOC, re-arranging Eqs. (3) with (4) gives:

$$\Delta\text{CO}_2 = \frac{(\text{DIC}_0 - \text{DIC}_t) - (\text{TOC}_t - \text{TOC}_0)}{2}. \quad (5)$$

Because TOC data were not available, we estimated the TOC generation indirectly from total inorganic nitrogen (TIN) consumption. Assuming the molar C:N ratio in freshwater being higher than the Redfield ratio of 106:16 [43, 44], TOC production could be estimated from the consumption of nitrate and ammonium, which are the main species of nitrogen in the groundwater system with nitrate accounting for the majority, based on a C:N ratio of 10:1 [45]. We assume that denitrification as a process that removes N from the system can be neglected in our case, because our system was turbulent and well aerated.

Our mass balance was calculated by multiplying the concentrations with the varying water volume in the setup (mesocosm bottom area \times decreasing water level

with negligible volume of the water in pipes and pump), so the evaporation would not influence our result.

We performed a series of analysis of variance (ANOVA) to explore the patterns of DIC, TOC, and CO₂ and their relationship to nutrient and flow velocity. The concentration of CO₂ at given DIC and alkalinity was calculated using standard dissociation constants of the carbonate system [46]. Data were log-transformed to satisfy assumptions of residuals normal distribution. ANOVA was applied to test for overall statistical differences among treatments. The ratio to the initial amount of the above parameters for each of the mesocosm was carried out to test for the treatment effects using ANOVA. In the model, nutrient and flow velocity were treated as the fixed effect, and temporal pseudo-replication from repeated sampling over time was considered as nested within each mesocosm as random effects. The comparison of DIC and CO₂ changes is given by the different slope of a first-order reaction of log₁₀ DIC or log₁₀ CO₂ over time to test for statistical differences for each treatment and mesocosm. All calculations, statistical analysis, and data visualization were performed using R version 3.5.1 [47].

Results

Significant differences among four treatments

The differences of flow velocities and nutrients among the four treatments were significant at the beginning of the experiment (Table 2). The nitrate concentration was similar between high and low flow with a larger variation range in high flow treatments. Because of some clogging of the pumps, the flow velocity fluctuated at a larger range at high flow compared to the low flow velocity.

At first, DO saturation increased exponentially over time in all mesocosms (Fig. 2). The initial DO concentration at high flow was higher than that at low flow at the starting time, probably because more turbulences at

high flow mixed more oxygen into the water before the first sampling. DO saturation varied dissimilarly over time and treatments as well. Mesocosms with nutrient additions developed a clear over-saturation, showing that TOC production was stimulated by nutrient additions. The A + L treatment reached the highest over-saturation. On the contrary, the control mesocosms rapidly reached equilibrium with atmosphere. As expected, equilibration was faster at high flow.

EC in the high flow velocity treatments showed a similar trend with a sharp decrease from 2.24 to 1.95 mS cm⁻¹ in the first 150 h after which it stayed constant (Fig. 2). The low flow velocity treatments showed a steadily decrease from 2.24 to 1.95 mS cm⁻¹ from the start to the end of experiment.

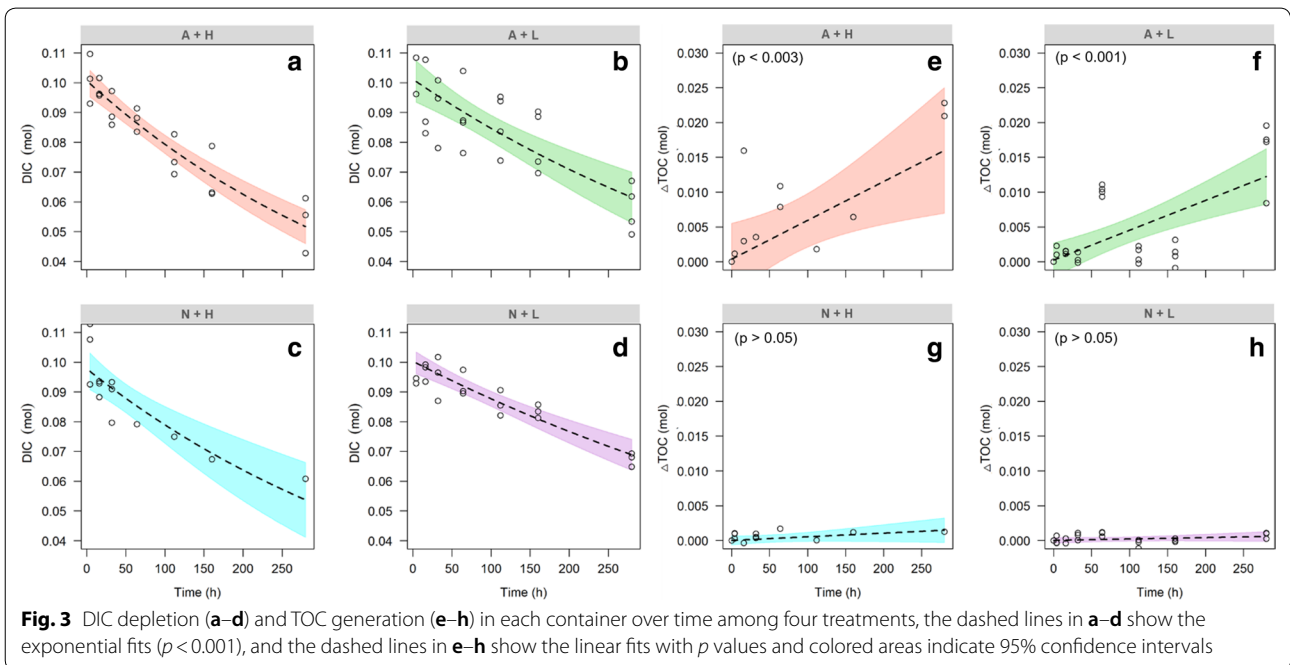
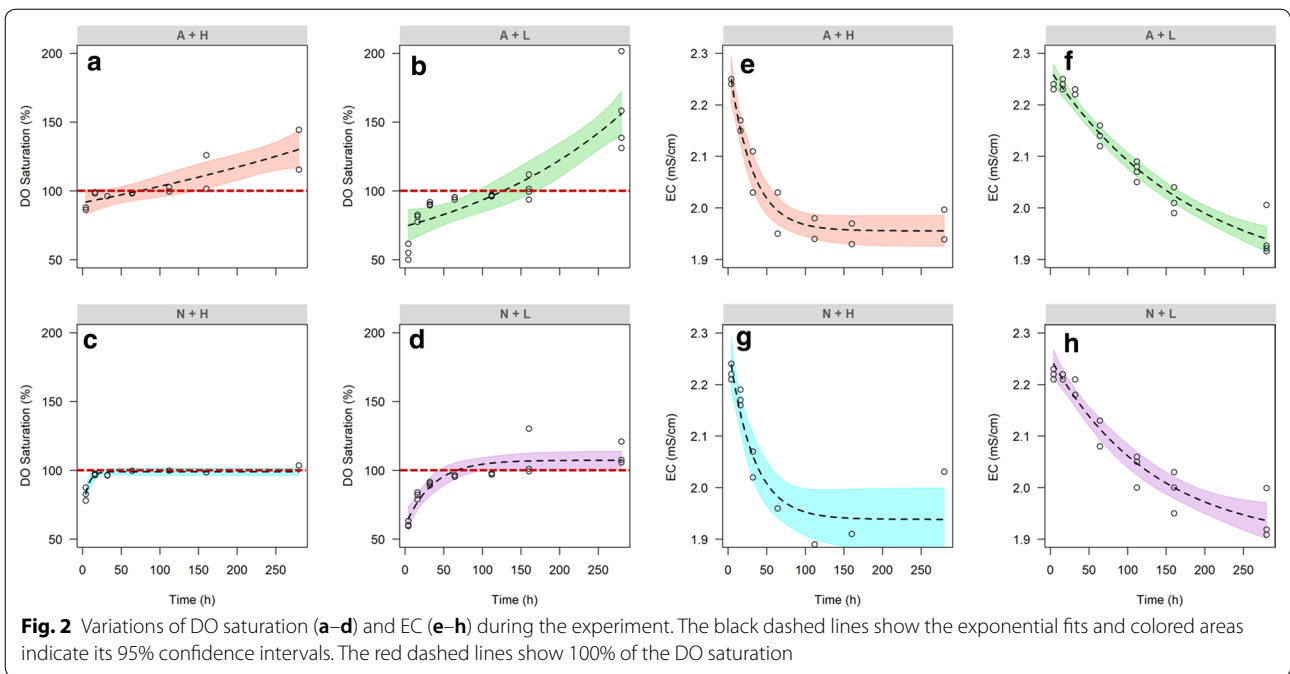
DIC and alkalinity were used to calculate the CO₂ concentrations at the beginning and in the end. At the end of the experiment in the high nutrient treatment, *p*CO₂ in water was below that in the atmosphere, indicating CO₂ uptake. Assuming alkalinity has a linear decrease over time accompanied with known DIC changes (Fig. 3a–d), we calculated the *p*CO₂ at any time in each mesocosm using the CO2SYS program [48]. Thus, the time when *p*CO₂ in each mesocosm was equal to *p*CO₂ in the atmosphere (*p*CO_{2air} = 395 μatm) could be estimated. After about 125 and 235 h, the systems switched to CO₂ uptake under the A + H and A + L treatments, respectively (Additional file 1: Figure S2). The N + L treatment reached CO₂ equilibration with atmosphere until the end of experiment.

DIC and TOC

The DIC amount in all treatments decreased continuously by 31–48% during the experimental period (Fig. 3). Decrease of DIC was largest in the A + H treatment and lowest in the N + L treatment. The amount of DIC in the system was significantly different between the two

Table 2 Flow velocities and chemical parameters at start (*t* = 0 h) and the end (*t* = 280 h) of the experiment among four treatments

Treatment	Abbreviation	Flow velocity (m s ⁻¹)	Time (h)	NO ₃ ⁻ -N concentration (mg L ⁻¹)	NH ₄ ⁺ -N concentration (μg L ⁻¹)	DIC concentration (mg L ⁻¹)	Alkalinity (μmol L ⁻¹)	<i>p</i> CO ₂ (μatm)
Add + high	A + H	0.37 ± 0.21	0	0.33 ± 0.01	5.6 ± 0.4	9.53 ± 4.79	721.2 ± 83.8	3537 ± 2670
			280	0.06 ± 0.07	0.03 ± 0.03	6.21 ± 3.18	571.2 ± 14.5	43.3 ± 34.8
Add + low	A + L	0.11 ± 0.07	0	0.33 ± 0.03	6.3 ± 1.2	10.11 ± 5.06	794.8 ± 17.0	3270 ± 2259
			280	0.13 ± 0.05	0.11 ± 0.12	6.40 ± 0.86	629.3 ± 60.4	439 ± 612
Non + high	N + H	0.32 ± 0.22	0	0.01 ± 0.01	6.2 ± 1.6	9.85 ± 4.94	758.3 ± 53.0	1889 ± 1349
			280	0.01 ± 0.00	0.01 ± 0.00	7.02 ± 3.51	588.9 ± 22.1	15.2 ± 15.8
Non + low	N + L	0.09 ± 0.06	0	0.02 ± 0.00	5.8 ± 0.9	9.33 ± 4.78	719.6 ± 81.9	3549 ± 1943
			280	0.01 ± 0.00	0.03 ± 0.05	7.25 ± 3.64	591.1 ± 25.1	383 ± 605



nutrient treatments ($p = 0.041$), as well as between the two flow velocities ($p = 0.020$). DIC in the N+H treatment decreased rapidly at the beginning of the experiment (particularly at the first 50 h). The decreasing rate of DIC under the A+H treatment surpassed that under the N+H treatment, while the rate was relatively slow but steadily after 170 h. The rate of DIC decrease was

also strongly related to flow velocity ($p = 0.006$) but had insignificant relationship with nutrients. Moreover, there was a significant interaction of flow velocity and nutrients in the DIC decrease slope showing a combined effect between the two factors ($p = 0.043$).

The TOC increase in the high nutrient treatments was evidently much higher than the one in the treatment

without nutrients addition (Fig. 3) and independent of flow velocity. In the low nutrient treatments, TOC did not significantly change during the experiment, indicating little TOC production in these systems. This is consistent with the DO data which showed no O₂ over-saturation in the low nutrient treatments (Fig. 2).

CO₂ evasions among four treatments

All mesocosms were net sources of CO₂ during the experimental period (Fig. 4). Always positive fluxes (except at the end of the experiment) were confirmed by our floating chamber measurements (Fig. 4e–h). The high flow treatments reached CO₂ equilibrium between water and atmosphere faster (Additional file 1: Figure S2). The rate of CO₂ change also shows the significant difference between flow velocity treatments ($p=0.024$). High flow velocity sped up CO₂ evasion. More CO₂ was emitted significantly under the high flow velocity ($p=0.005$) and low nutrient condition ($p=0.096$). CO₂ emission from the low nutrient treatments was 35% higher than that in the high nutrient treatments in average.

CO₂ evasions of the N+H treatment increased rapidly during the first 80 h, and remained nearly constant after 150 h. The A+H treatment emitted markedly a lot of CO₂ at the beginning but the flux became lower over time. CO₂ evasion from the two low flow treatments exhibited a similar behavior with relatively gentle and steady CO₂ emissions, and the N+L treatment released evidently more CO₂ than the A+L treatment.

Combined with the result of $p\text{CO}_2$ changes (Additional file 1: Figure S2), CO₂ uptake could occur by the time when $p\text{CO}_2$ concentration dropped below $p\text{CO}_{2\text{air}}$. The floating chamber measurement also showed that some CO₂ was taken up (CO₂ flux < 0) under the high nutrient treatments at the time of 280 h. The rate of CO₂ uptake can be calculated from $p\text{CO}_2$ and the gas transfer velocity (k_{600}):

$$f_{\text{CO}_2} = k_{600} \cdot k_{\text{H}} \cdot (p\text{CO}_2 - p\text{CO}_{2\text{air}}). \quad (6)$$

k_{H} is Henry's constant for CO₂ at a given temperature and salinity [49]. Gas transfer velocity (k_{600}) could be calculated from the initial DIC depletion in the low nutrient treatments assuming that there was little TOC produced in these systems (Fig. 3g, h). Assuming k_{600} being constant and equivalent under the same flow velocity treatments, k_{600} was 0.93 and 0.23 m day⁻¹ in the high and low flow velocity treatments, respectively. Using these k_{600} values and the final $p\text{CO}_2$ we can calculate the CO₂ flux at the end of the experiment using Eq. (6). Multiplying that flux with the duration of the under-saturated period results in an average total CO₂ uptake of 42 and 9.5 μmol in the A+H and A+L treatments, respectively. This is much lower than the observed changes in DIC. Thus, uptake did not significantly contribute to the total C budget of the experiment (Fig. 4).

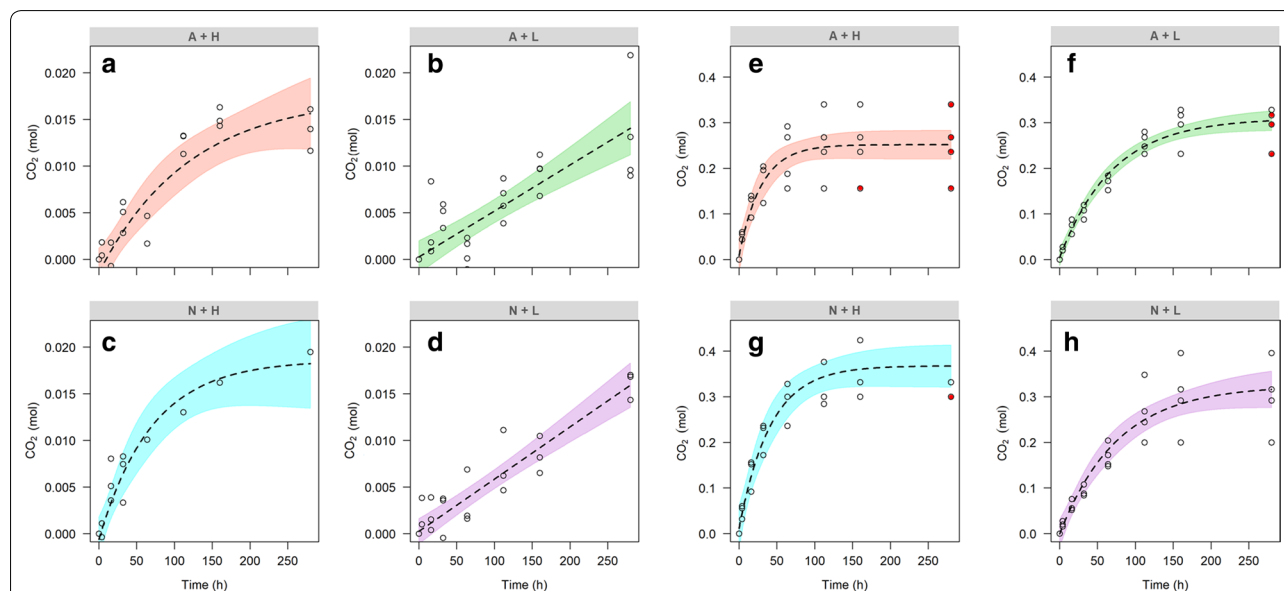


Fig. 4 Cumulative CO₂ emissions in each container over time among four treatments calculated from DIC (a–d) and from floating chamber measurements (e–h), the dashed lines show the exponential fits ($p < 0.001$) and colored areas indicate 95% confidence level, the red dots indicate the negative CO₂ fluxes, namely there was CO₂ uptake occurring

Discussion

Carbon dynamics

Our results show that flow velocity and nutrient level determine the rate and amount of CO₂ evasion, respectively. CO₂ evasion depends on both CO₂ concentration and the gas transport coefficient (k) in Eq. (6) [50, 51]. With the CO₂ evasions under the same flow treatments showing similar tendency over time, flow velocity altered k , which determined the rate of CO₂ emission. Meanwhile, treatments with the same nutrient level ended with similar amount of CO₂ evasion, suggesting that the nutrient level ultimately dictates the quantity of CO₂ emission. Providing that more TOC was generated in the high nutrient treatment, our results confirm that TOC generation reallocate the depletion of inorganic carbon.

Our results also highlight the interaction of the flow and nutrient speeding up the depletion rate of DIC in drainage channels ($p=0.043$). However, there was no significant synergistic effect of velocity and nutrients on the final DIC amount remaining in the system ($p=0.40$). Flow velocity significantly altered the slope of DIC and CO₂ over time, indicating that flow velocity dominated the rate of DIC consumption and CO₂ emissions. Simultaneously, flow velocity influences the quantity of DIC consumption as well, possibly by means of regulating on ecosystem metabolism. High flow can intensify the capacity of an ecosystem to store and process carbon [52]. TOC production at high flow velocity could be enhanced by higher light and nutrient availability throughout the water column due to better mixing [53]. Low flow on the other hand may promote sedimentation, thereby improving water clarity which may increase TOC production [33]. Nutrients affect the quantity of both CO₂ and DIC by altering the pattern of the inorganic carbon utilization through ecosystem processes (i.e., gross primary production, ecosystem respiration) [54, 55]. Nutrient enrichment may accelerate TOC processing, transformation, and export, potentially altering food-web dynamics and ecosystem stability in the long term [54]. Higher water temperature enhances photosynthesis enzyme activity that favors the biomass growth [56]. In our study, the synergy of both factors cannot be explained by light availability or temperature, because turbidity was low due to lack of sediment and temperature did not differ between treatments (mean water temperature of 25.0 ± 1.0 °C within each sampling). Most probable, better mixing at high flow prevented possible local nutrient limitation of photosynthesis in our experiment.

Uncertainty

Effects of C:N ratio on carbon budgets

Our TOC results are sensitive towards the chosen C:N ratio (10:1 in our case). We examined the responsiveness of the C:N ratio to the DIC allocation in our experiment by calculating carbon mass balances for different C:N ratios [C:N=5, 106:16 (Redfield ratio), 10 (used in this study), and 15] (Additional file 1: Figure S3). Variation of the C:N ratio changed the absolute amount of CO₂ emitted from the high nutrient treatments but did not change the general pattern.

Alkalinity dynamics

In a closed system changes in alkalinity only occur by processes including either a solid phase or conversion to a gas, which then escapes to the atmosphere [57]. Beside the definition of the alkalinity as acid neutralizing capacity of a solution titrated to the CO₂ equivalence point, the alkalinity can be also described by the equivalent sum of conservative cations (those that do not affect alkalinity) minus the sum of conservative anions:

$$\begin{aligned} \text{Alkalinity} = & [\text{Na}^+] + [\text{K}^+] + 2[\text{Mg}^{2+}] \\ & + 2[\text{Ca}^{2+}] + 2[\text{Mn}^{2+}] + [\text{NH}_4^+] \\ & + 2[\text{Fe}^{2+}] - [\text{Cl}^-] - 2[\text{SO}_4^{2-}] - [\text{NO}_3^-]. \end{aligned} \quad (7)$$

The changes of alkalinity caused by nitrate and ammonium consumption can account for 0.1–26.2% of the total alkalinity variation. The continuous EC decline during the experiment (Fig. 2) was also observed indicating that not only nitrogen transformation occurred, but there was also ion precipitation inducing alkalinity dropping down. The main ions in the groundwater were SO₄²⁻, HCO₃⁻ (affects the DIC change), Na⁺, and Ca²⁺ [58]. Chemical theory predicts that upon evaporation, half of the bicarbonate in the groundwater will re-equilibrate with the atmosphere releasing CO₂ while the other half precipitates, mostly as calcite [11]. Thus, calcite precipitation must have affected our $p\text{CO}_2$ calculations and led to alkalinity decrease through Ca²⁺ removal from the system. Assuming the measured alkalinity changes ($153 \mu\text{mol L}^{-1}$ in average) were completely caused by calcite precipitation, then there would be $77 \mu\text{mol L}^{-1}$ Ca²⁺ being utilized for CaCO₃ formed in each mesocosm. This is roughly consistent with our CO₂ emission calculations, because assuming one calcite formed per emitted CO₂ would result in 69–168 $\mu\text{mol L}^{-1}$ Ca²⁺ being utilized for CaCO₃ formed.

Method uncertainties in CO₂ flux measurement

We used two methods to quantify CO₂ emissions during our experiments: a carbon budget approach and direct flux measurements using floating chambers. Theoretically, the cumulative CO₂ flux measured by the chamber should match the cumulative C loss from the water,

$$S \int_0^t f(t) dt = (c_t - c_0)V, \tag{8}$$

where *S* is the surface area of the water; *f*(*t*) is the CO₂ emission flux as a function of time; *V* is the volume of the water, *c*₀ and *c*_{*t*} are the CO₂ concentrations at time 0 and *t*, respectively.

We found that the results of the direct flux measurement and the DIC calculation were not consistent. The flux chamber method resulted in a twenty-time overestimation of the CO₂ evasion especially at higher flow (Fig. 4). This is likely because of the artificial turbulence generated by the floating chamber [59, 60]. Deployment of floating chamber in the mesocosm system could cause a large overestimation of the CO₂ evasion compared with the one in natural waters [61, 62], which

would lead to an unrealistic carbon budget with all carbon removed from the system by outgassing in our carbon budget. Thus, floating chamber measurements cannot be used to quantify CO₂ emissions in flume experiments.

Implications and upscaling

Drainage channels receive irrigation water from agriculture and route the nutrient containing groundwater directly into streams. High flow velocity accelerates the CO₂ evasion to the atmosphere rapidly (Fig. 5), leaving less opportunity for channel metabolism and processing [32]. Previous research also suggests that CO₂ concentrations are largely reduced by intensive primary production in rivers [63]. Thus, nutrient additions have the potential to attenuate CO₂ emissions. The formed biomass is transported downstream and could be trapped in lentic parts of the drainage network, where particle sedimentation mainly occurs. Notably, collected particulate carbon needs to be properly buried or dredged. Otherwise methane production is likely to take place in the sediment accumulations. That would largely increase the GHG effect of the drainage network due to the larger global

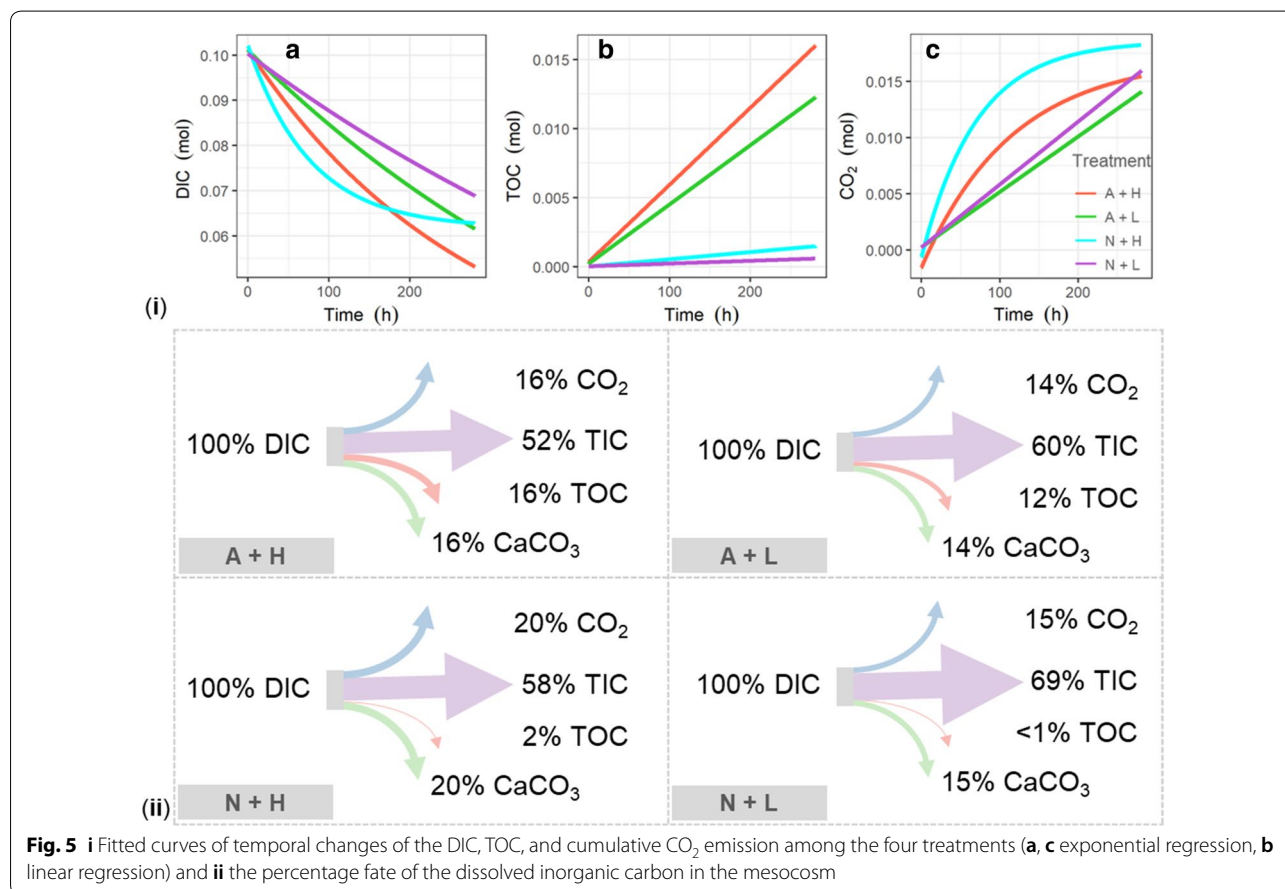


Fig. 5 i Fitted curves of temporal changes of the DIC, TOC, and cumulative CO₂ emission among the four treatments (a, c exponential regression, b linear regression) and ii the percentage fate of the dissolved inorganic carbon in the mesocosm

warming potential of methane compared to CO₂ [21, 30]. Alternatively, in-stream plankton could potentially be mineralized by heterotrophic respiration [19, 64]. In that case, CO₂ would only be temporarily bound and later liberated further downstream.

At a given rate of CO₂ emission, the flow velocity determines the required distance until the CO₂ concentration in a drainage ditch equilibrates with the atmosphere. In a hypothetical drainage system of infinite length with no biological processes involved, it could be anticipated that the only fate of inorganic carbon is to outgas into atmosphere. Our study suggest that up to 20% of DIC would be converted to CO₂ and 58% of the initial DIC would be transported downstream considering no other processes were involved until the *p*CO₂ in the water equilibrates with the atmosphere. Previous study reported large variations of the release rate of atmospheric carbon from rivers to the atmosphere (2–30%) [65]. From field measurements of GHG emissions, Ran et al. [66] concluded that 35% of the carbon exported into the Yellow River network was degassed from the entire watershed during fluvial transport, which is comparable with our estimation.

Irrigation in the study area mainly occurs in March–April (to ensure the water requirement of winter-wheat during the growth period), and October (before wheat sowing). In the case of extreme drought in summer, irrigation is also needed for maize growth in July or August. During other periods the water residence time in the agricultural drainage is quite long, because runoff in irrigated agriculture is mainly related to the intensity of irrigation and rainfall events in comparison to the infiltration capacity of the soil [67]. In NCP, the streamflow has dramatically decreased because of the human activities. Low level of groundwater and large evaporation potential in this semi-arid region often lead to lentic water in drainages [68]. High primary production in the stagnant drainage channels will make them a carbon sink.

The median bicarbonate concentration of aquifer systems in the NCP is approximately 241 mg L⁻¹ based on representative samples from three plain types [36]. Using the conservative assumption that when groundwater reaches the surface, half of the bicarbonate (121 mg L⁻¹) is converted to CO₂ [11] which is equivalent to 87 mg L⁻¹ CO₂. Annual groundwater net depletion in NCP was estimated as a volume of 8.3 ± 1.1 km³ year⁻¹ [7]. The estimated annual CO₂ emissions due to groundwater depletion in the NCP are thus approximately 0.52 ± 0.07 Mt (1 Mt = 10¹² g). The irrigation efficiency in this region is about 0.5 as reported earlier [69]. Thus, half of the pumped groundwater reaches the drainage channels. However, we do not know how much of the CO₂ is set free already on the fields and which part of it is entering the drainage channels. Furthermore, no biological carbon fixation is considered. This makes our estimate a worst case scenario. Indeed, high CO₂ emissions during irrigation the fields have been observed [70]. Agriculture is always an integrative practice with soil management, fertilization, and irrigation. Further studies are needed to understand how much groundwater CO₂ is emitted during the agricultural management and how much ends up in the drainage channels.

Groundwater depletion in the NCP contributed a great number of CO₂ which is quite close to the groundwater CO₂ efflux in US and India (Table 3), and accounted for ~5% of the global groundwater extraction. CO₂ released from groundwater depletion has not yet been included in the Chinese carbon inventory [71]. A previous study indicates that groundwater loss in the NCP was approximately 50 km³ within 8 years, which is greater than the capacity of China's Three Gorges Dam (39.3 km³), the world's largest power station [7]. Thus, CO₂ emissions from groundwater pumping should be considered in global carbon budgets [72, 73]. This is especially relevant, because groundwater depletion is expected to acceleration in the future [74].

Table 3 Comparison of CO₂ emissions from groundwater pumping in the NCP with other regions of the world as well as with other CO₂ sources in the NCP

CO ₂ emissions	Description	References
9.7–13.5 Mt CO ₂ year ⁻¹	Groundwater irrigation global estimate	[11]
~ 10 Mt C year ⁻¹	Global groundwater extraction	[9]
~ 0.72 Mt CO ₂ year ⁻¹	Groundwater irrigation in India	[73]
1.7 Mt CO ₂ year ⁻¹	Groundwater irrigation in the US	[11]
0.52 ± 0.07 Mt CO ₂ year ⁻¹	Groundwater depletion in the NCP	This study
8.72 Mt CO ₂ e year ⁻¹	GHG emissions of energy use for irrigation water pumping in the NCP	[75]
120.87 Mt CO ₂ e year ⁻¹	GHG emissions from agricultural production process in the NCP by life cycle assessment	[76]
121 Mt CO ₂ year ⁻¹	CO ₂ emissions from central heating supply due to natural gas usage in the NCP	[77]
15.99 Mt CO ₂ year ⁻¹	Crop burning emissions during harvest seasons in the NCP	[78]

Conclusions

Up to now, carbon dioxide emissions from irrigation drainage networks remain poorly understood. Mesocosm experiments help to unravel the effect of different drivers by experimental manipulation and replications. Here, we applied controlled mesocosm experiments to investigate the impact of flow velocity and nutrients on carbon dynamics in irrigation groundwater entering drainage channels in an intensive agricultural landscape. High nutrients contributed to TOC generation and in turn reduce CO₂ evasion on a short term. High flow velocity, on the other hand, promoted rapid CO₂ evasion at high nutrient level. Overall, TOC production counteracted CO₂ evasion, whereas both of the flow velocity and nutrients stimulate DIC depletion. For a proper quantification of the real CO₂ emissions from the entire network, information about flow velocity and residence time of the water in the ditch network as well as information about the fate of organic matter formed in the ditches is necessary. Controlled mesocosm experiments are a useful tool to disentangle the interaction of the various processes involved.

Supplementary information

Supplementary information accompanies this paper at <https://doi.org/10.1186/s12302-020-00426-2>.

Additional file 1. Supplementary materials.

Acknowledgements

We thank colleagues from Department of Lake Research in Helmholtz Center for Environmental Research for valuable discussion.

Authors' contributions

PL and FL designed the mesocosm experiment. PL, KD, and ZL were involved in performing the mesocosm experiment and collecting the samples. PL, CG, and MK analyzed and interpreted the data. PL drafted the manuscript. MK contributed to the study design and revised the manuscript. All authors read and approved the final manuscript.

Funding

This work was supported by the National Natural Science Foundation of China (NSFC) No. 41771292. P. Leng is supported by the CAS-DAAD Joint Fellowship Program for Doctoral Students.

Availability of data and materials

The data of this article can be found online at https://figshare.com/articles/Raw_Data_xlsx/9874394.

Ethics approval and consent to participate

Not applicable.

Consent for publication

Not applicable.

Competing interests

The authors declare that they have no competing interests.

Author details

¹ Key Laboratory of Ecosystem Network Observation and Modeling, Institute of Geographic and Natural Resources Research, Chinese Academy of Sciences, Beijing, China. ² Department of Lake Research, Helmholtz Centre

for Environmental Research-UFZ, Magdeburg, Germany. ³ College of Resources and Environment, University of Chinese Academy of Sciences, Beijing, China.

Received: 4 August 2020 Accepted: 21 October 2020

Published online: 31 October 2020

References

- Giordano M (2009) Global groundwater? Issues and solutions. *Annu Rev Environ Resour* 34(1):153–178. <https://doi.org/10.1146/annurev.envir.030308.100251>
- Siebert S, Burke J, Faures JM, Frenken K, Hoogeveen J, Döll P, Portmann FT (2010) Groundwater use for irrigation—a global inventory. *Hydrol Earth Syst Sci* 14(10):1863–1880. <https://doi.org/10.5194/hess-14-1863-2010>
- Famiglietti JS (2014) The global groundwater crisis. *Nat Clim Change* 4:945. <https://doi.org/10.1038/nclimate2425>
- de Graaf IEM, Gleeson T, van Beek LPH, Sutanudjaja EH, Bierkens MFP (2019) Environmental flow limits to global groundwater pumping. *Nature* 574(7776):90–94. <https://doi.org/10.1038/s41586-019-1594-4>
- Wang J, Rothausen SGSA, Conway D, Zhang L, Xiong W, Holman IP, Li Y (2012) China's water–energy nexus: greenhouse-gas emissions from groundwater use for agriculture. *Environ Res Lett* 7(1):014035. <https://doi.org/10.1088/1748-9326/7/1/014035>
- Zhu X, Li Y, Li M, Pan Y, Shi P (2013) Agricultural irrigation in China. *J Soil Water Conserv* 68(6):147A–154A. <https://doi.org/10.2489/jswc.68.6.147A>
- Feng W, Zhong M, Lemoine J-M, Biancale R, Hsu H-T, Xia J (2013) Evaluation of groundwater depletion in North China using the Gravity Recovery and Climate Experiment (GRACE) data and ground-based measurements. *Water Resour Res* 49(4):2110–2118. <https://doi.org/10.1002/wrcr.20192>
- Jahangir MMR, Johnston P, Khalil MI, Hennessy D, Humphreys J, Fenton O, Richards KG (2012) Groundwater: a pathway for terrestrial C and N losses and indirect greenhouse gas emissions. *Agric Ecosyst Environ* 159:40–48. <https://doi.org/10.1016/j.agee.2012.06.015>
- Macpherson GL (2009) CO₂ distribution in groundwater and the impact of groundwater extraction on the global C cycle. *Chem Geol* 264(1):328–336. <https://doi.org/10.1016/j.chemgeo.2009.03.018>
- Borges AV, Darchambeau F, Lambert T, Bouillon S, Morana C, Brouyère S, Hakoun V, Jurado A, Tseng HC, Descy JP, Roland FAE (2018) Effects of agricultural land use on fluvial carbon dioxide, methane and nitrous oxide concentrations in a large European river, the Meuse (Belgium). *Sci Total Environ* 610–611:342–355. <https://doi.org/10.1016/j.scitotenv.2017.08.047>
- Wood WW, Hyndman DW (2017) Groundwater depletion: a significant unreported source of atmospheric carbon dioxide. *Earth's Future* 5(11):1133–1135. <https://doi.org/10.1002/2017EF000586>
- McGill BM, Hamilton SK, Millar N, Robertson GP (2018) The greenhouse gas cost of agricultural intensification with groundwater irrigation in a Midwest US row cropping system. *Glob Change Biol* 24(12):5948–5960. <https://doi.org/10.1111/gcb.14472>
- Myhre G, Shindell D, Bréon FM, Collins W, Fuglestedt J, Huang J, Koch D, Lamarque JF, Lee D, Mendoza B, Nakajima T, Robock A, Stephens G, Takemura T, Zhang H (2013) Climate change 2013: the physical science basis: contribution of Working Group I to the Fifth Assessment. Cambridge University Press, Cambridge
- Liang LL, Grantz DA, Jenerette GD (2016) Multivariate regulation of soil CO₂ and N₂O pulse emissions from agricultural soils. *Glob Change Biol* 22(3):1286–1298. <https://doi.org/10.1111/gcb.13130>
- Houghton RA, House JJ, Pongratz J, van der Werf GR, DeFries RS, Hansen MC, Le Quééré C, Ramankutty N (2012) Carbon emissions from land use and land-cover change. *Biogeosciences* 9(12):5125–5142. <https://doi.org/10.5194/bg-9-5125-2012>
- West TO, Marland G (2003) Net carbon flux from agriculture: carbon emissions, carbon sequestration, crop yield, and land-use change. *Biogeochemistry* 63(1):73–83. <https://doi.org/10.1023/a:1023394024790>
- Zamanian K, Zarebanadkouki M, Kuzyakov Y (2018) Nitrogen fertilization raises CO₂ efflux from inorganic carbon: a global assessment. *Glob Change Biol* 24(7):2810–2817. <https://doi.org/10.1111/gcb.14148>
- Butman D, Stackpole S, Stets E, McDonald CP, Clow DW, Striegl RG (2016) Aquatic carbon cycling in the conterminous United States and implications for terrestrial carbon accounting. *Proc Natl Acad Sci* 113(1):58–63. <https://doi.org/10.1073/pnas.1512651112>

19. Hotchkiss ER, Hall RO Jr, Sponseller RA, Butman D, Klaminder J, Laudon H, Rosvall M, Karlsson J (2015) Sources of and processes controlling CO₂ emissions change with the size of streams and rivers. *Nat Geosci* 8:696. <https://doi.org/10.1038/ngeo2507>
20. Koschorreck M, Downing AS, Hejzlar J, Marcé R, Laas A, Arndt WG, Keller PS, Smolders AJP, van Dijk G, Kosten S (2019) Hidden treasures: human-made aquatic ecosystems harbour unexplored opportunities. *Ambio*. <https://doi.org/10.1007/s13280-019-01199-6>
21. Schrier-Uijl AP, Veraart AJ, Leffelaar BA, Berendse F, Veenendaal EM (2011) Release of CO₂ and CH₄ from lakes and drainage ditches in temperate wetlands. *Biogeochemistry* 102(1):265–279. <https://doi.org/10.1007/s10533-010-9440-7>
22. Stumm W, Morgan JJ (2012) *Aquatic chemistry: chemical equilibria and rates in natural waters*, vol 126. Wiley, New York
23. Duvert C, Bossa M, Tyler KJ, Wynn JG, Munksgaard NC, Bird MI, Setterfield SA, Hutley LB (2019) Groundwater-derived DIC and carbonate buffering enhance fluvial CO₂ evasion in two Australian Tropical Rivers. *J Geophys Res Biogeosci* 124(2):312–327. <https://doi.org/10.1029/2018jg004912>
24. Cole JJ, Prairie YT, Caraco NF, McDowell WH, Tranvik LJ, Striegl RG, Duarte CM, Kortelainen P, Downing JA, Middelburg JJ (2007) Plumbing the global carbon cycle: integrating inland waters into the terrestrial carbon budget. *Ecosystems* 10(1):172–185. <https://doi.org/10.1007/s10021-006-9013-8>
25. Borges AV, Darchambeau F, Teodoru CR, Marwick TR, Tamooh F, Geeraert N, Omengo FO, Guerin F, Lambert T, Morana C, Okuku E, Bouillon S (2015) Globally significant greenhouse-gas emissions from African inland waters. *Nat Geosci* 8(8):637–642. <https://doi.org/10.1038/ngeo2486>
26. Raymond PA, Hartmann J, Lauerwald R, Sobek S, McDonald C, Hoover M, Butman D, Striegl R, Mayorga E, Humborg C, Kortelainen P, Durr H, Meybeck M, Ciais P, Guth P (2013) Global carbon dioxide emissions from inland waters. *Nature* 503(7476):355–359. <https://doi.org/10.1038/nature12760>
27. Halbedel S, Koschorreck M (2013) Regulation of CO₂ emissions from temperate streams and reservoirs. *Biogeosciences* 10(11):7539–7551. <https://doi.org/10.5194/bg-10-7539-2013>
28. Borges AV, Darchambeau F, Lambert T, Morana C, Allen GH, Tambwe E, Toengaho Sembaito A, Mambo T, Nlandu Wabakhangazi J, Descy JP, Teodoru CR, Bouillon S (2019) Variations in dissolved greenhouse gases (CO₂, CH₄, N₂O) in the Congo River network overwhelmingly driven by fluvial-wetland connectivity. *Biogeosciences* 16(19):3801–3834. <https://doi.org/10.5194/bg-16-3801-2019>
29. Dinsmore KJ, Billett MF, Dyson KE (2013) Temperature and precipitation drive temporal variability in aquatic carbon and GHG concentrations and fluxes in a peatland catchment. *Glob Change Biol* 19(7):2133–2148. <https://doi.org/10.1111/gcb.12209>
30. Gómez-Gener L, Obrador B, von Schiller D, Marcé R, Casas-Ruiz JP, Proia L, Acuña V, Catalán N, Muñoz I, Koschorreck M (2015) Hot spots for carbon emissions from Mediterranean fluvial networks during summer drought. *Biogeochemistry* 125(3):409–426. <https://doi.org/10.1007/s10533-015-0139-7>
31. Liu S, Lu XX, Xia X, Yang X, Ran L (2017) Hydrological and geomorphological control on CO₂ outgassing from low-gradient large rivers: an example of the Yangtze River system. *J Hydrol* 550:26–41. <https://doi.org/10.1016/j.jhydrol.2017.04.044>
32. Liu S, Raymond PA (2018) Hydrologic controls on pCO₂ and CO₂ efflux in US streams and rivers. *Limnol Oceanogr Lett* 3(6):428–435. <https://doi.org/10.1002/lol2.10095>
33. Crawford JT, Loken LC, Stanley EH, Stets EG, Dornblaser MM, Striegl RG (2016) Basin scale controls on CO₂ and CH₄ emissions from the Upper Mississippi River. *Geophys Res Lett* 43(5):1973–1979. <https://doi.org/10.1002/2015GL067599>
34. Zhao X, Li F, Ai Z, Li J, Gu C (2018) Stable isotope evidences for identifying crop water uptake in a typical winter wheat–summer maize rotation field in the North China Plain. *Sci Total Environ* 618:121–131. <https://doi.org/10.1016/j.scitotenv.2017.10.315>
35. Zhou Z, Zhang G, Yan M, Wang J (2012) Spatial variability of the shallow groundwater level and its chemistry characteristics in the low plain around the Bohai Sea, North China. *Environ Monit Assess* 184(6):3697–3710. <https://doi.org/10.1007/s10661-011-2217-1>
36. Chen Z, Nie Z, Zhang Z, Qi J, Nan Y (2005) Isotopes and sustainability of ground water resources, North China Plain. *Groundwater* 43(4):485–493. <https://doi.org/10.1111/j.1745-6584.2005.0038.x>
37. Zhang Y, Li F, Li J, Liu Q, Tu C, Suzuki Y, Huang C (2015) Spatial distribution, potential sources, and risk assessment of trace metals of groundwater in the North China Plain. *Hum Ecol Risk Assess* 21(3):726–743. <https://doi.org/10.1080/10807039.2014.921533>
38. Shao J, Ling Y, Zhang Z (2013) Groundwater flow simulation and its application in groundwater resource evaluation in the North China Plain, China. *Acta Geol Sin* 87(1):243–253. <https://doi.org/10.1111/1755-6724.12045>
39. Petersen JE, Kemp WM, Bartleson R, Boynton WR, Chen C-C, Cornwell JC, Gardner RH, Hinkle DC, Houde ED, Malone TC (2003) Multiscale experiments in coastal ecology: improving realism and advancing theory. *Bioscience* 53(12):1181–1197. [https://doi.org/10.1641/0006-3568\(2003\)053\[1181:MEICE\]2.0.CO;2](https://doi.org/10.1641/0006-3568(2003)053[1181:MEICE]2.0.CO;2)
40. Liboriussen L, Landkildehus F, Meerhoff M, Bramm ME, Søndergaard M, Christoffersen K, Richardson K, Søndergaard M, Lauridsen TL, Jeppesen E (2005) Global warming: design of a flow-through Shallow Lake mesocosm climate experiment. *Limnol Oceanogr Methods* 3(1):1–9. <https://doi.org/10.4319/lom.2005.3.1>
41. Parkhurst DL, Appelo C (2013) Description of input and examples for PHREEQC version 3: a computer program for speciation, batch-reaction, one-dimensional transport, and inverse geochemical calculations. US Geological Survey
42. Li J, Li F, Liu Q, Zhang Y (2014) Trace metal in surface water and groundwater and its transfer in a Yellow River alluvial fan: evidence from isotopes and hydrochemistry. *Sci Total Environ* 472:979–988. <https://doi.org/10.1016/j.scitotenv.2013.11.120>
43. Hecky RE, Campbell P, Hendzel LL (1993) The stoichiometry of carbon, nitrogen, and phosphorus in particulate matter of lakes and oceans. *Limnol Oceanogr* 38(4):709–724. <https://doi.org/10.4319/lo.1993.38.4.0709>
44. They NH, Amado AM, Cotner JB (2017) Redfield ratios in inland waters: higher biological control of C:N:P ratios in tropical semi-arid high water residence time lakes. *Front Microbiol* 8:1505–1505. <https://doi.org/10.3389/fmicb.2017.01505>
45. Stubbins A (2016) A carbon for every nitrogen. *Proc Natl Acad Sci* 113(39):10736–10738. <https://doi.org/10.1073/pnas.1612995113>
46. Zeebe RE, Wolf-Gladrow D (2001) CO₂ in seawater: equilibrium, kinetics, isotopes, vol 65. Gulf Professional Publishing, Amsterdam
47. R Core Team (2019) A language and environment for statistical computing. R Foundation for Statistical Computing, Vienna, Austria. <https://www.R-project.org>
48. Lewis E, Wallace D, Allison LJ (1998) Program developed for CO₂ system calculations. Brookhaven National Lab., Dept. of Applied Science, Upton, NY (United States)
49. Weiss RF (1974) Carbon dioxide in water and seawater: the solubility of a non-ideal gas. *Mar Chem* 2(3):203–215. [https://doi.org/10.1016/0304-4203\(74\)90015-2](https://doi.org/10.1016/0304-4203(74)90015-2)
50. Alin SR, de Fátima FLRM, Salimon CI, Richey JE, Holtgrieve GW, Krusche AV, Snidvongs A (2011) Physical controls on carbon dioxide transfer velocity and flux in low-gradient river systems and implications for regional carbon budgets. *J Geophys Res Biogeosci*. <https://doi.org/10.1029/2010JG001398>
51. Raymond PA, Zappa CJ, Butman D, Bott TL, Potter J, Mulholland P, Laursen AE, McDowell WH, Newbold D (2012) Scaling the gas transfer velocity and hydraulic geometry in streams and small rivers. *Limnol Oceanogr* 57(1):41–53. <https://doi.org/10.1215/21573689-1597669>
52. Aristi I, Arroita M, Larrañaga A, Ponsati L, Sabater S, von Schiller D, Elosegi A, Acuña V (2014) Flow regulation by dams affects ecosystem metabolism in Mediterranean rivers. *Freshw Biol* 59(9):1816–1829. <https://doi.org/10.1111/fwb.12385>
53. Moss BR (2009) *Ecology of fresh waters: man and medium, past to future*. Wiley, New York
54. Benstead JP, Rosemond AD, Cross WF, Wallace JB, Eggert SL, Suberkropp K, Gulis V, Greenwood JL, Tant CJ (2009) Nutrient enrichment alters storage and fluxes of detritus in a headwater stream ecosystem. *Ecology* 90(9):2556–2566. <https://doi.org/10.1890/08-0862.1>
55. Williamson TJ, Cross WF, Benstead JP, Gíslason GM, Hood JM, Huryan AD, Johnson PW, Welter JR (2016) Warming alters coupled carbon and

- nutrient cycles in experimental streams. *Glob Change Biol* 22(6):2152–2164. <https://doi.org/10.1111/gcb.13205>
56. Hall RO Jr, Yackulic CB, Kennedy TA, Yard MD, Rosi-Marshall EJ, Voichick N, Behn KE (2015) Turbidity, light, temperature, and hydropeaking control primary productivity in the Colorado River, Grand Canyon. *Limnol Oceanogr* 60(2):512–526. <https://doi.org/10.1002/lno.10031>
 57. Koschorreck M, Tittel J (2007) Natural alkalinity generation in neutral lakes affected by acid mine drainage. *J Environ Qual* 36(4):1163–1171. <https://doi.org/10.2134/jeq2006.0354>
 58. Zhang F, Li F, Li J, Shuai S, Cai W, Chang C (2013) Hydrochemical characteristics of surface water in main rivers of the irrigation districts in the downstream of Yellow River. *Acta Autom Sin* 21(4):487–493. <https://doi.org/10.3724/SPJ.1011.2013.00487>
 59. Lorke A, Bodmer P, Noss C, Alshboul Z, Koschorreck M, Somlaihaase C, Bastviken D, Flury S, McGinnis DF, Maeck A (2015) Technical note: drifting versus anchored flux chambers for measuring greenhouse gas emissions from running waters. *Biogeosciences* 12(23):7013–7024. <https://doi.org/10.5194/bg-12-7013-2015>
 60. Raymond PA, Cole JJ (2001) Gas exchange in rivers and Estuaries: choosing a gas transfer velocity. *Estuaries* 24(2):312–317. <https://doi.org/10.2307/1352954>
 61. Marino R, Howarth RW (1993) Atmospheric oxygen exchange in the Hudson River: dome measurements and comparison with other natural waters. *Estuaries* 16(3):433–445. <https://doi.org/10.2307/1352591>
 62. Vachon D, Prairie YT, Cole JJ (2010) The relationship between near-surface turbulence and gas transfer velocity in freshwater systems and its implications for floating chamber measurements of gas exchange. *Limnol Oceanogr* 55(4):1723–1732. <https://doi.org/10.4319/lno.2010.55.4.1723>
 63. Houser JN, Bartsch LA, Richardson WB, Rogala JT, Sullivan JF (2015) Ecosystem metabolism and nutrient dynamics in the main channel and backwaters of the Upper Mississippi River. *Freshw Biol* 60(9):1863–1879. <https://doi.org/10.1111/fwb.12617>
 64. Vannote RL, Minshall GW, Cummins KW, Sedell JR, Cushing CE (1980) The river continuum concept. *Can J Fish Aquat Sci* 37(1):130–137. <https://doi.org/10.1139/f80-017>
 65. Li S, Lu XX, He M, Zhou Y, Li L, Ziegler AD (2012) Daily CO₂ partial pressure and CO₂ outgassing in the upper Yangtze River basin: a case study of the Longchuan River, China. *J Hydrol* 466:141–150. <https://doi.org/10.1016/j.jhydrol.2012.08.011>
 66. Ran L, Lu XX, Yang H, Li L, Yu R, Sun H, Han J (2015) CO₂ outgassing from the Yellow River network and its implications for riverine carbon cycle. *J Geophys Res Biogeosci* 120(7):1334–1347. <https://doi.org/10.1002/2015jg002982>
 67. Foster S, Pulido-Bosch A, Vallejos Á, Molina L, Llop A, MacDonald AM (2018) Impact of irrigated agriculture on groundwater-recharge salinity: a major sustainability concern in semi-arid regions. *Hydrogeol J* 26(8):2781–2791. <https://doi.org/10.1007/s10040-018-1830-2>
 68. Varis O, Vakkilainen P (2001) China's 8 challenges to water resources management in the first quarter of the 21st century. *Geomorphology* 41(2):93–104. [https://doi.org/10.1016/S0169-555X\(01\)00107-6](https://doi.org/10.1016/S0169-555X(01)00107-6)
 69. Qu SS, Zhu ZZ, Qiu N, Wang WP (2012) The impact of irrigation diverting from Yellow River water on regional water cycle in Shandong Province. *Appl Mech Mater* 212–213:514–517. <https://doi.org/10.4028/www.scientific.net/AMM.212-213.514>
 70. Tang J, Wang J, Li Z, Wang S, Qu Y (2018) Effects of irrigation regime and nitrogen fertilizer management on CH₄, N₂O and CO₂ emissions from saline-alkaline paddy fields in Northeast China. *Sustainability* 10(2):475. <https://doi.org/10.3390/su10020475>
 71. Shan Y, Guan D, Zheng H, Ou J, Li Y, Meng J, Mi Z, Liu Z, Zhang Q (2018) China CO₂ emission accounts 1997–2015. *Sci Data* 5:170201. <https://doi.org/10.1038/sdata.2017.201>
 72. Currell MJ, Cartwright I, Bradley DC, Han D (2010) Recharge history and controls on groundwater quality in the Yuncheng Basin, North China. *J Hydrol* 385(1):216–229. <https://doi.org/10.1016/j.jhydrol.2010.02.022>
 73. Mishra V, Asoka A, Vatta K, Lall U (2018) Groundwater depletion and associated CO₂ emissions in India. *Earth's Future* 6(12):1672–1681. <https://doi.org/10.1029/2018ef000939>
 74. Zhao Q, Zhang B, Yao Y, Wu W, Meng G, Chen Q (2019) Geodetic and hydrological measurements reveal the recent acceleration of groundwater depletion in North China Plain. *J Hydrol* 575:1065–1072. <https://doi.org/10.1016/j.jhydrol.2019.06.016>
 75. Qiu GY, Zhang X, Yu X, Zou Z (2018) The increasing effects in energy and GHG emission caused by groundwater level declines in North China's main food production plain. *Agric Water Manag* 203:138–150. <https://doi.org/10.1016/j.agwat.2018.03.003>
 76. Zhang X (2019) Multiple cropping system expansion: increasing agricultural greenhouse gas emissions in the north China plain and neighboring regions. *Sustainability* 11(14):3941. <https://doi.org/10.3390/su11143941>
 77. Cui Y, Zhang W, Wang C, Streets DG, Xu Y, Du M, Lin J (2019) Spatiotemporal dynamics of CO₂ emissions from central heating supply in the North China Plain over 2012–2016 due to natural gas usage. *Appl Energy* 241:245–256. <https://doi.org/10.1016/j.apenergy.2019.03.060>
 78. Liu M, Song Y, Yao H, Kang Y, Li M, Huang X, Hu M (2015) Estimating emissions from agricultural fires in the North China Plain based on MODIS fire radiative power. *Atmos Environ* 112:326–334. <https://doi.org/10.1016/j.atmosenv.2015.04.058>

Publisher's Note

Springer Nature remains neutral with regard to jurisdictional claims in published maps and institutional affiliations.

Submit your manuscript to a SpringerOpen® journal and benefit from:

- Convenient online submission
- Rigorous peer review
- Open access: articles freely available online
- High visibility within the field
- Retaining the copyright to your article

Submit your next manuscript at ► [springeropen.com](https://www.springeropen.com)